Electronic Supplementary Material (ESI) for Journal of Materials Chemistry C.
This journal is © The Royal Society of Chemistry 2021

Supporting Information

Few-Layered Two-Dimensional Molecular Crystals for Organic Artificial Visual Memories with Record-High Photoresponse

Lijuan Zhang,[a] Xinzi Tian,[a] Jiarong Yao,[a] Xianneng Song,[a] Shuyuan Yang,[a] Siyu Guo,[a] Ying Wang,[a] Bin Li,[a] Xiaochen Ren,[a] Yan Sun,[a] Fangxu Yang,[a] Rongjin Li*[a] and Wenping Hu[a,b]

Experimental Section

2DMCs Growth and transfer

C8-BTBT was dissolved in toluene at a concentration of 1 mg mL^{-1}. The surfactant sodium perfluorooctanoate was also added into the toluene solution (~0.001 mg·mL^{-1}) to enhance spreading for growth of ultrathin 2DMCs. Glass weighing bottles (60 mm × 30 mm) were used as growth containers for the C8-BTBT 2DMCs. The bottles were cleaned by sonification in ethanol for 30 min. As a liquid substrate for crystal growth, 20 mL of glycerol was added into the weighing bottle. Next, 50 μL of C8-BTBT solution (1 mg mL^{-1} in toluene) was slowly dropped on the glycerol surface and the bottle was then placed in a cabinet with constant temperature and humidity (typical temperature of 10°C and humidity of ~60%). After the solvent evaporated completely, C8-BTBT 2DMCs floating on the surface of glycerol were obtained. SiO_2 (300 nm)/Si wafer substrates were successively cleaned by sonification in deionized (DI) water, acetone, and isopropanol for 10 min. The substrates were then treated with oxygen plasma at 80 W for 10 min followed by immediate modification with PTS using a vapor phase method. The PTS-modified SiO_2/Si substrates were successively cleaned by sonification in chloroform, n-hexane, and isopropanol for 10 min. The 2DMCs floating on the surface of the glycerol were transferred to the PTS-modified SiO_2/Si substrates by dipping the substrate upside down on the glycerol surface and fishing out the crystals. The SiO_2/Si substrate with C8-BTBT 2DMCs was gently rinsed using DI water to remove excess glycerol and surfactant. C6-DPA and C10-BTBT 2DMCs were grown and transferred using the same method.

Device Fabrication

Bottom-gate/top-contact devices were fabricated on the PTS-modified SiO_2/Si substrates by stamping Au (80 nm) stripes on C8-BTBT 2DMCs for source and drain electrodes. The mobility of the OFETs in the saturation regime was calculated from the following equation: $I_{ds} = (W/2L)\mu C_i (V_{gs} - V_{th})^2$, where I_{ds} is the source–drain current, μ is the field-effect mobility, V_{th} is the threshold voltage, V_{gs} is the applied gate voltage, L is the channel length, W is the channel width, and the C_i is the specific capacitance (10 nF cm^{-2}).

Instrumentation

OM and POM images were obtained with Nikon ECLIPSE Ci-POL POMs with a blue filter. Intelligent mode AFM and KPFM images were measured using a Bruker Dimension Icon. XRD measurements were carried out in reflection mode at 45 kV and 200 mA with monochromatic Cu Kα radiation utilizing a Rigaku Smartlab diffractometer. UV–visible absorption spectra of C8-BTBT 2DMCs transferred onto a quartz substrate were measured with a SHZMADZU UV-3600 Plus spectrophotometer. Bright-field TEM images and corresponding SAED pattern measurements were conducted on a Tecnai G2 F20 S-TWIN TEM. The OFETs were measured using a Keithley 4200 SCS in ambient environment and using a TTPX Cryogenic probe station in vacuum at room temperature (approximately 20°C). The OPTs were measured using a laser with tunable power intensity. Laser power intensity was measured in situ with a PM100 digital power meter.

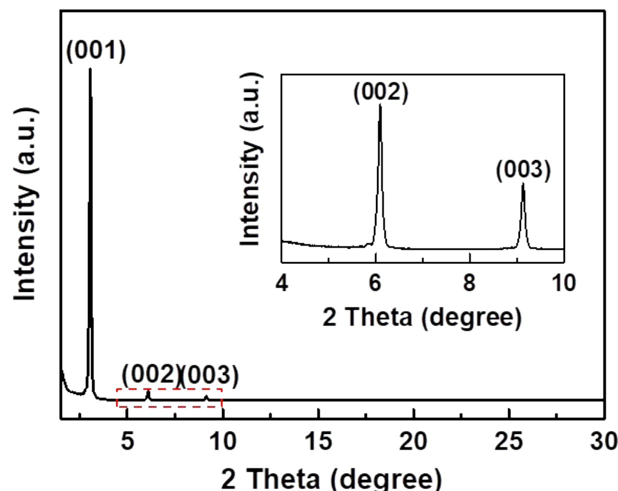

Fig. S1 XRD pattern of the C8-BTBT 2DMCs on SiO_2/Si substrates.

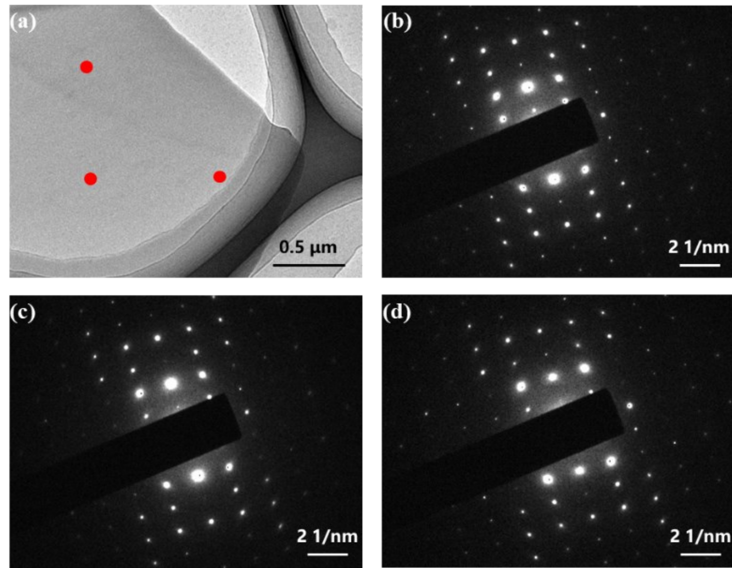

Fig. S2 TEM image and its corresponding SAED patterns of different positions of the 2DMCs sample.

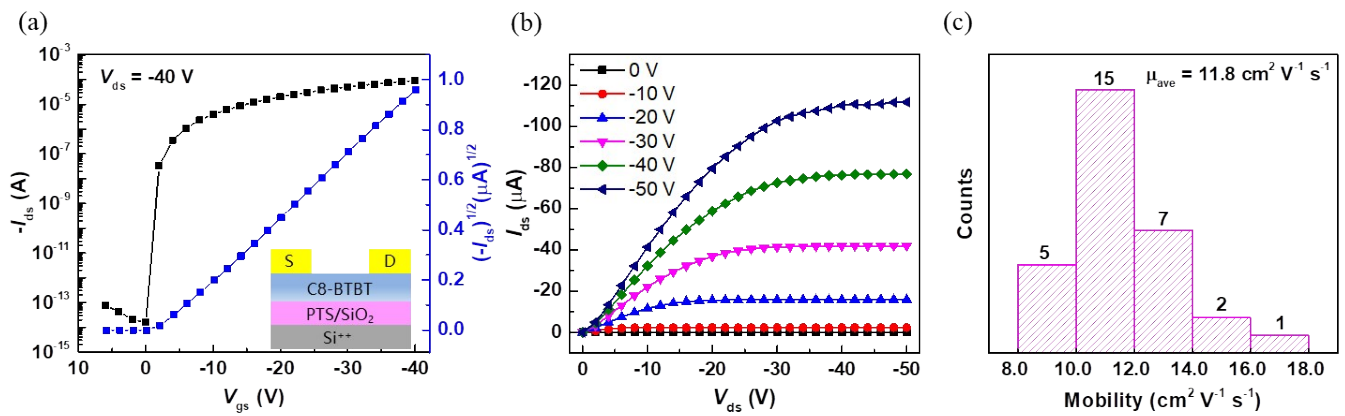

Fig. S3 Charge transport properties of the 2DMCs. (a) Typical transfer and (b) output characteristics curves of the OFETs based on 2DMCs of C8-BTBT (W/L = 1.52). (c) The mobility distribution of 30 devices.

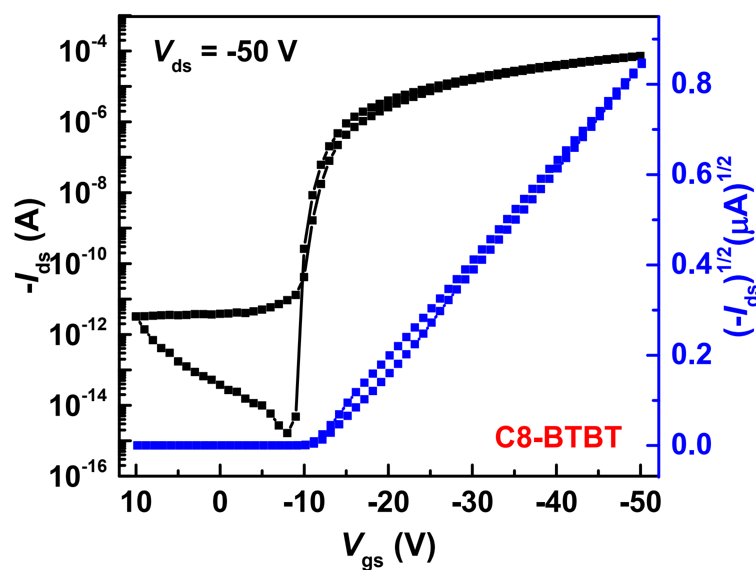

Fig. S4. The dual sweep for the transfer curve of the OFET based on C8-BTBT 2DMC in dark conditions.

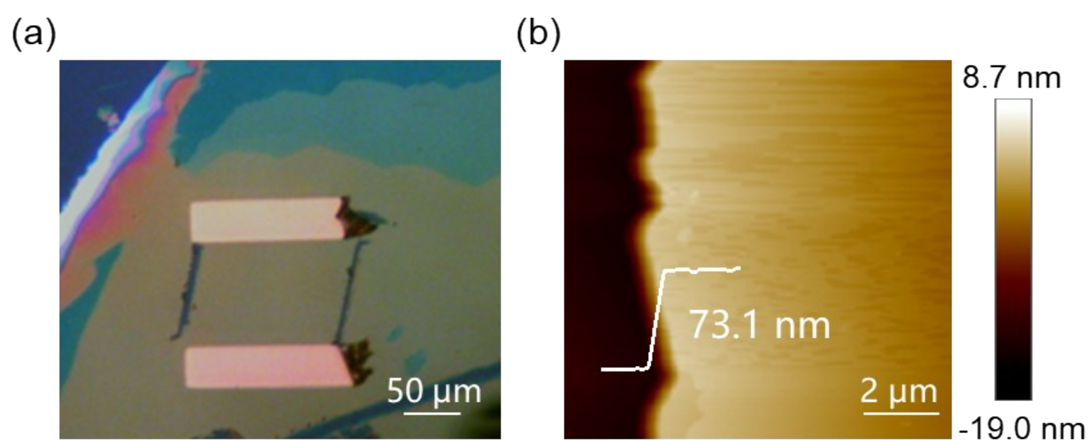

Fig. S5 The morphology of a thick crystal. (a) An OM image and (b) an AFM image of the thick C8-BTBT crystal.

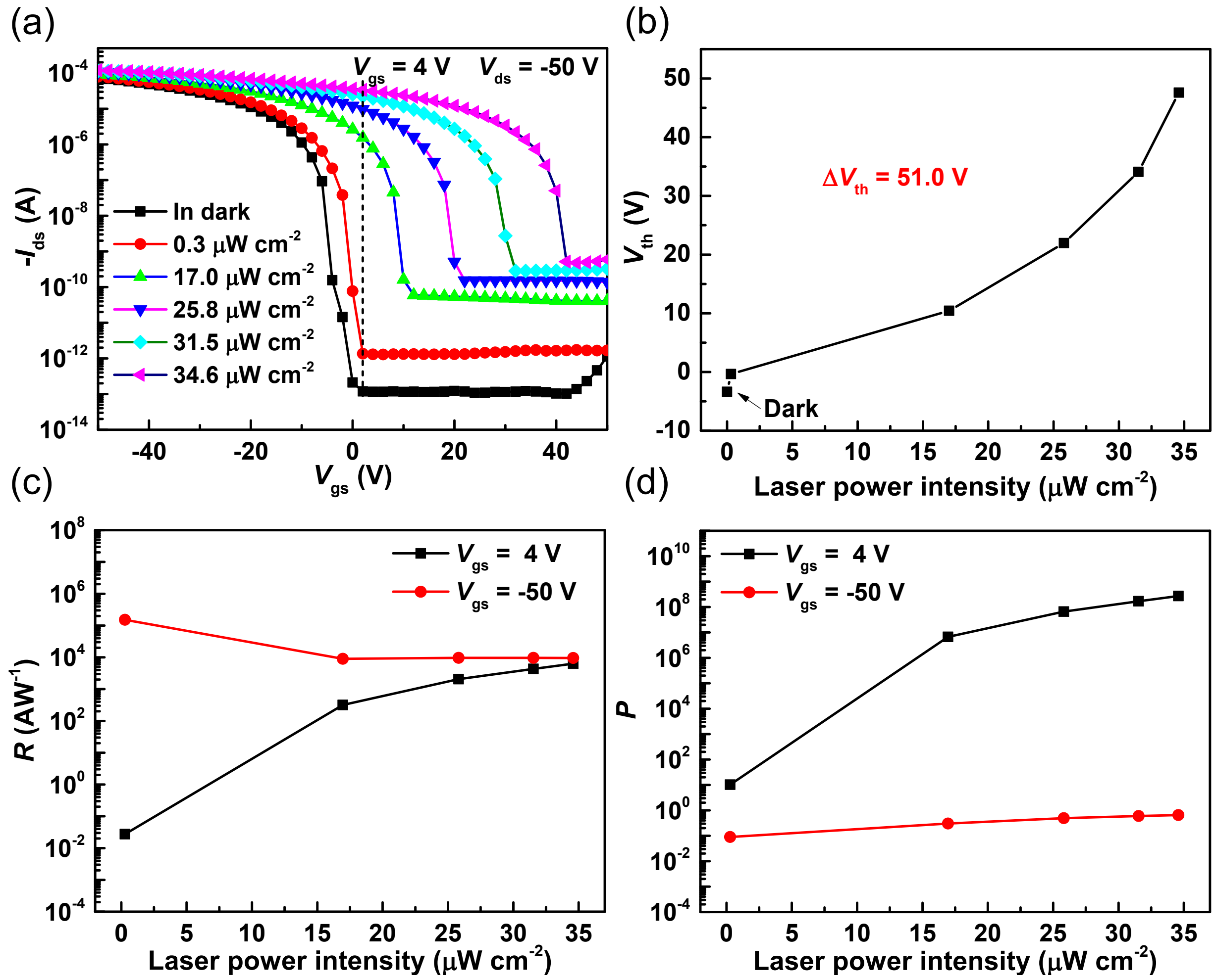

Fig. S6 Photodetection function of the AVMs based on a thick crystal as shown in Fig. S5. (a) Transfer curves of the device in dark and under laser irradiation of different power intensities. (b) Shift of V_{th} as a function of laser power intensity. (c) R, (d) P as a function of laser power intensity.

When a thick crystal with a thickness of 73.1 nm was used as the channel, the transfer curve shifted by increasing the laser power intensity from 0.3 to 34.6 μW cm^{-2}, and the maximum positive ΔV_{th} was 51.0 V (Figs. S6a and S6b), which was lower than the maximum positive ΔV_{th} (61.5 V, Fig. 2b) of the AVMs based on few-layers 2DMCs under similar measuring conditions. A maximum R of 1.5×10^5 A W^{-1} was obtained at V_{gs} = -50 V under incident laser power intensity of 0.3 μW cm^{-2} (Fig. S6c), maximum P reached 2.7×10^8 at V_{gs} = 4 V under laser power intensity of 34.6 μW cm^{-2} (Fig. S6d).

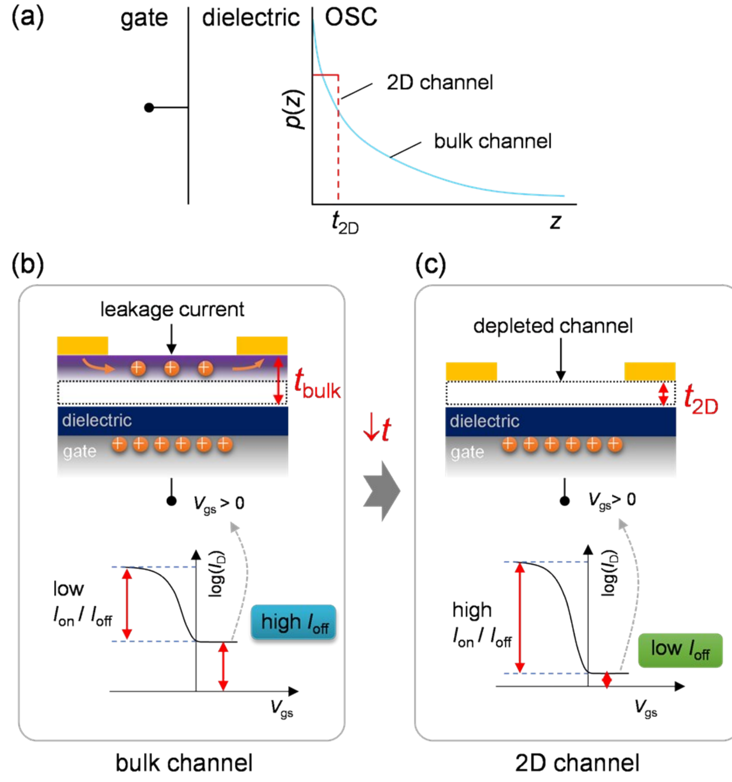

Fig. S7 Schematics showing the interlayer shielding effect. (a) Charge carrier density as a function of distance from the OSC/dielectric interface *z* in OFETs with a bulk and 2D channel.[1] (b) and (c) Infuence of Interlayer shielding effect in OFETs with (b) bulk or (c) 2D channel.[2]

The interlayer shielding effect is shown in Fig. S7 (taking a p-type OSC as an example). For an OFET based on a semi-infinitely thick channel with an exponential density of states (DOS), the hole density $p(z)$ along the direction perpendicular to the OSC/dielectric interface, z, is given by[1]

$$p(\mathrm{z}) = \frac{2k_{\mathrm{B}}T_0\varepsilon_0\varepsilon_{\mathrm{SC}}}{e^2(\mathrm{z}+\mathrm{z}_0)^2} \quad \cdots\cdots \ (1)$$

With

$$z_0 = \frac{2k_{\mathrm{B}}T_0\varepsilon_0\varepsilon_{\mathrm{SC}}}{eC_{\mathrm{i}}V_{\mathrm{x}}} \quad \cdots\cdots \ (2)$$

where $k_B T_0$ is the width of the exponential DOS, k_B is the Boltzmann constant, ε_0 is the vacuum permittivity, ε_{sc} is the dielectric constant of the semiconductor, C_i is the specific gate capacitance, e is the elementary charge, and V_x is the difference between the gate bias and the local channel potential at a point x in the channel. According to equations (1) and (2), $p(z)$ decreases with the square of z in a semi-infinitely thick channel (Fig. S7a bulk channel). The infinite thickness assumption is invalid for OFETs based on 2D OSCs. In this case, the carriers induced by the gate are confined in the 2D channel. The local hole density is described by[1]

$$p = \frac{C_{\mathrm{i}}V_{\mathrm{x}}}{et_{\mathrm{2D}}} \quad \cdots\cdots \ (3)$$

where t_{2D} is the thickness of the 2D OSC. According to equation (3), p is a constant and is proportional to gate voltage (Fig. S7a 2D channel). The value of t_{2D}, i.e. the thickness of the charge transporting layer in OFETs, was identified to be equal to the thickness of a few molecular layers.[3-5]

The I-V characteristics of OFETs with a bulk or 2D channel (Figs. S7b and S7c) can be explained by the different distribution of charge carrier density. Because of the 2D nature of the charge transporting layer in OFETs, for a bulk channel ($t_{ch} >> t_{2D}$), the hole density is not zero for $z > t_{2D}$. As result, interlayer shielding effect occurs and a positive gate voltage cannot fully deplete the channel. A leakage current occurs in the upper part of the bulk channel and the off current (I_{off}) is high (Fig. S7b); while for a 2D channel ($t_{ch} \leq t_{2D}$), the channel can be fully depleted, resulting in a low I_{off} (Fig. S7c).

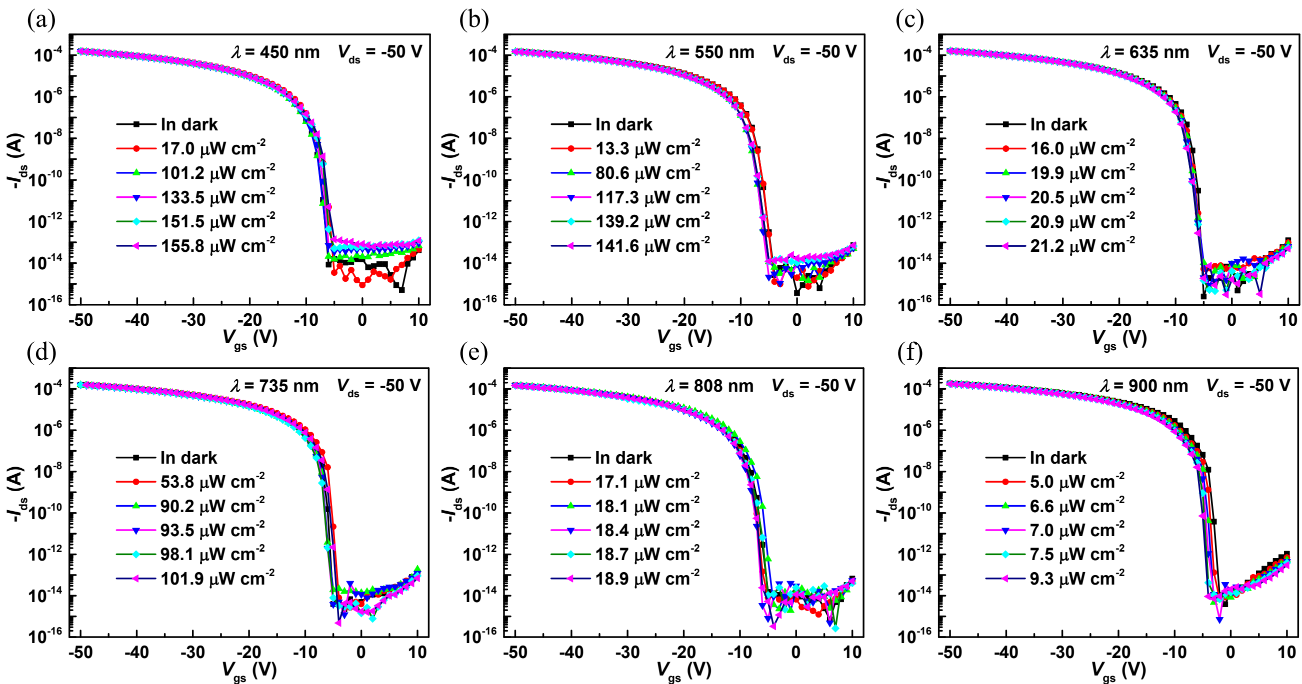

Fig. S8 Transfer curves of the device in dark and under laser irradiation of different power intensities and different wavelengths (400-900 nm).

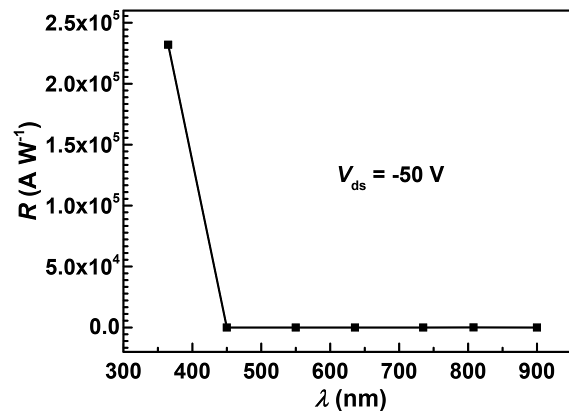

Fig. S9 R as a function of laser irradiation wavelengths (300 - 900 nm).

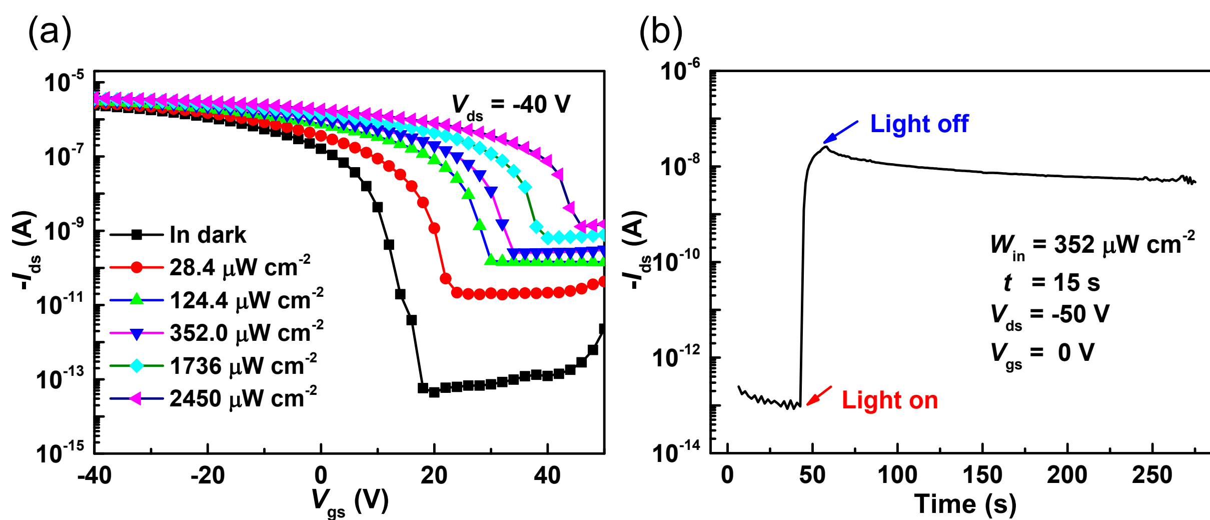

Fig. S10. (a) Transfer curves of the device based on C6-DPA 2DMCs in dark and under white light irradiation with different power intensities. (b) Retention time of the devices (V_{ds} = -50 V, V_{gs} = 0 V, white light 352 μW cm^{-2} for 15 s).

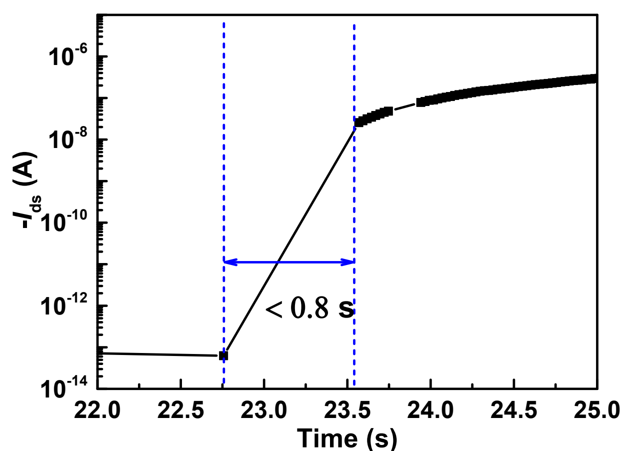

Fig. S11 The response time of the AVMs (384 μW cm^{-2} 365 nm UV light).

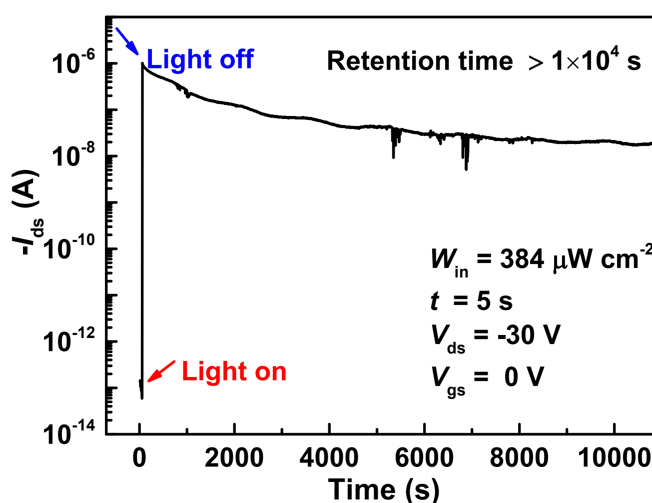

Fig. S12 Retention time (over 10^4 s) of the AVMs.

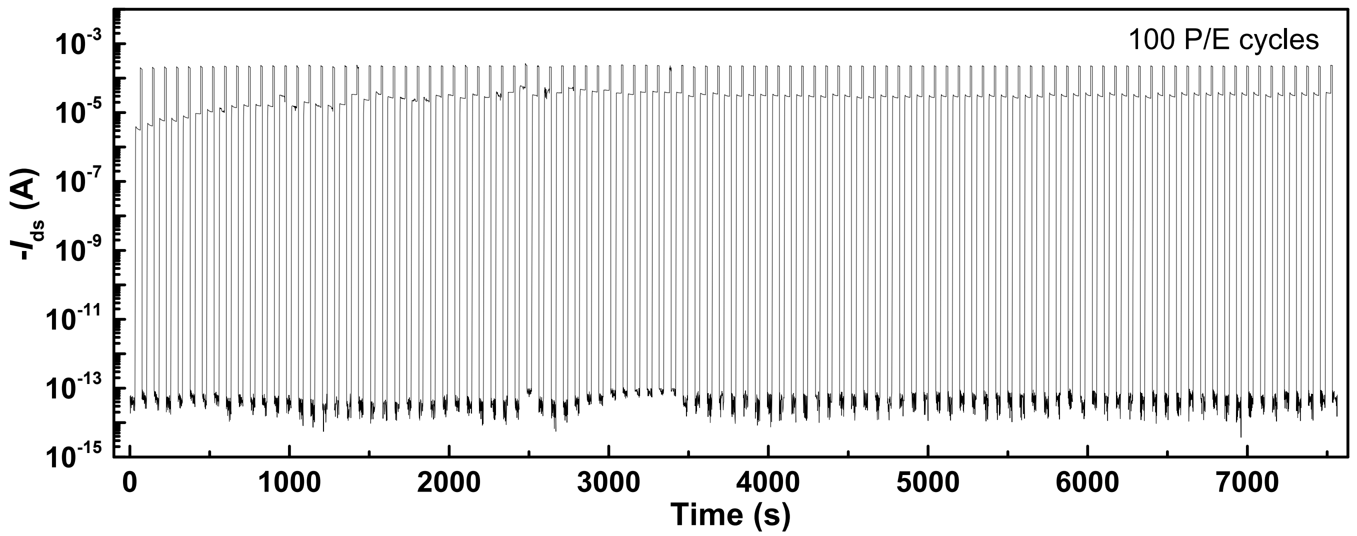

Fig. S13 The 100 P/E cycle test of the device.

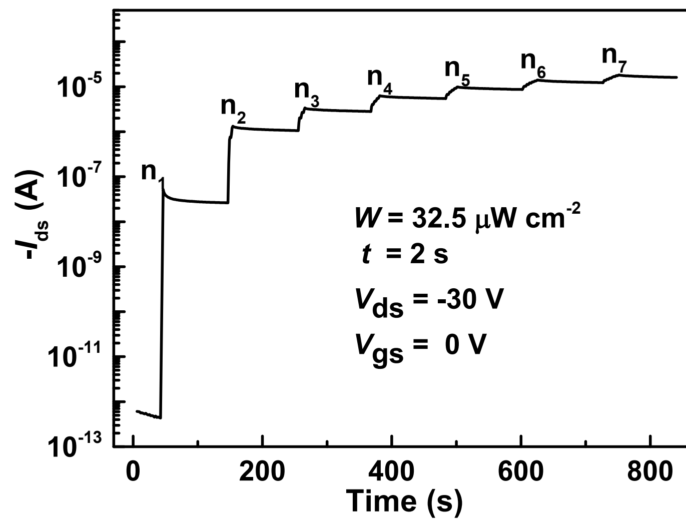

Fig. S14 Multiple distinct current levels obtained under different number of light irradiations with fixed light intensity and durations (laser power intensity fixed at 32.5 μW cm^{-2}, V_{gs} = 0 V).

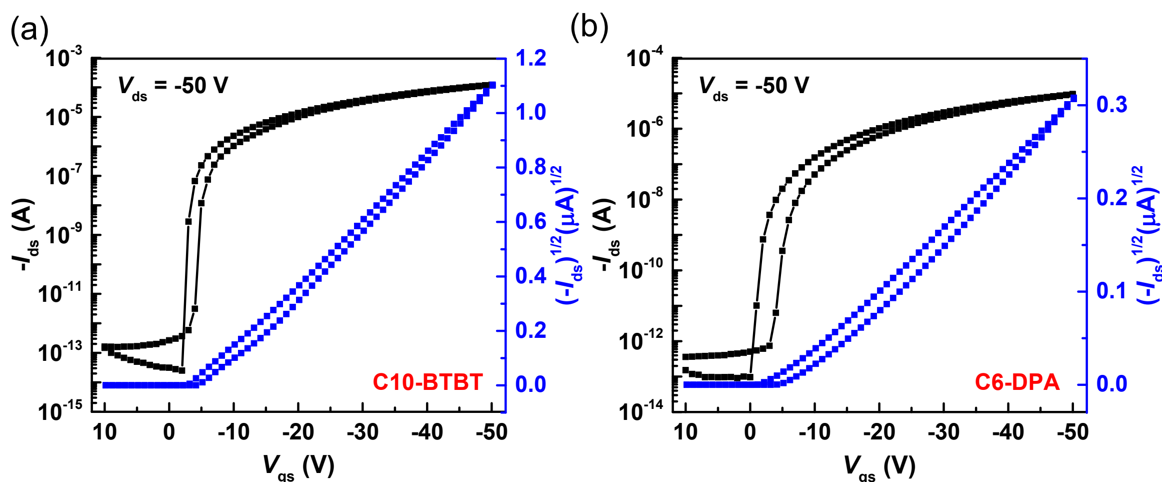

Fig. S15 The dual sweep for the transfer curves of the OFETs based on C10-BTBT and C6-DPA 2DMCs in dark conditions.

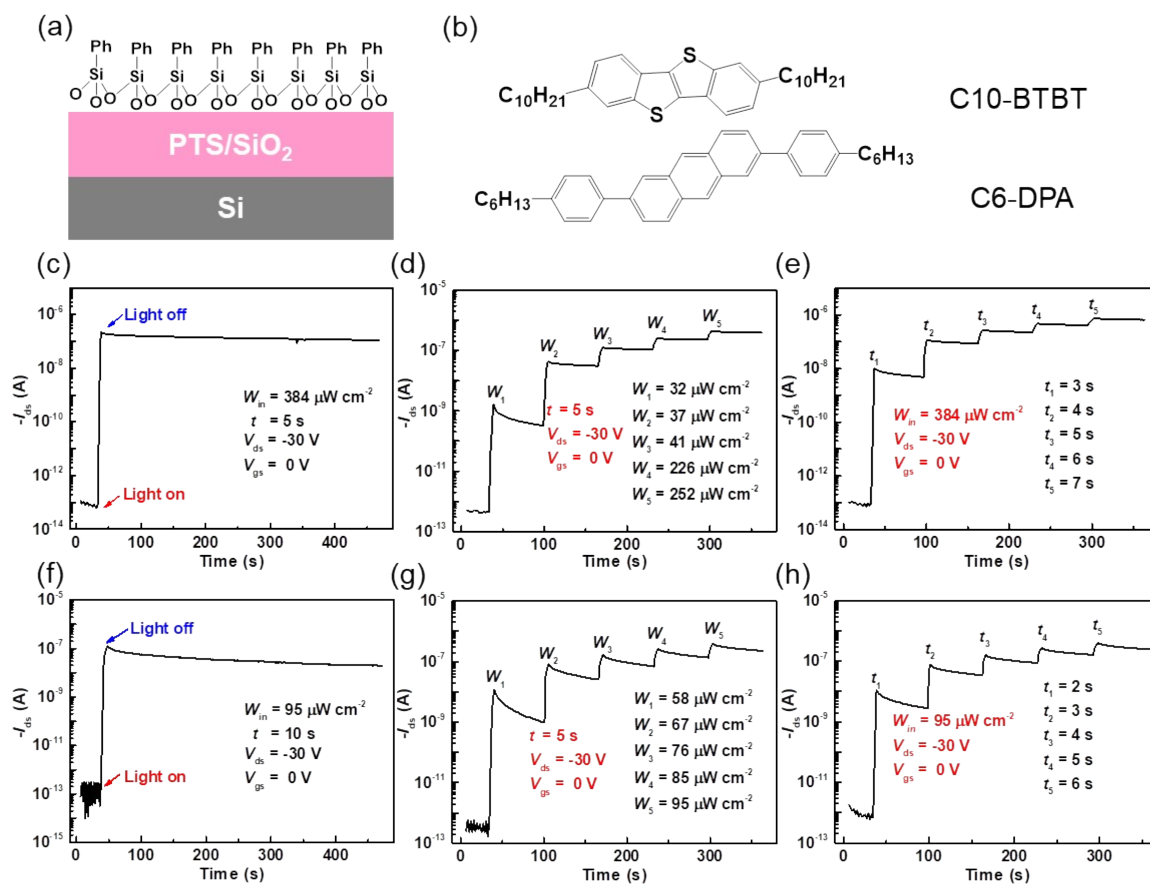

Fig. S16 Memory function of the AVMs based on different organic semiconductors. (a) The interface states of the PTS-modified SiO_2 substrates. (b) The molecular structures of two commonly used semiconductors C10-BTBT and C6-DPA. (c and f) Retention time of the AVMs based C10-BTBT and C6-DPA. (d and g) Multiple distinct levels obtained by laser irradiation of different intensities and (e and h) multiple distinct current levels obtained by laser irradiation of different time of the AVMs based C10-BTBT and C6-DPA (All tests were performed at V_{ds} = -30 V, V_{gs} = 0 V).

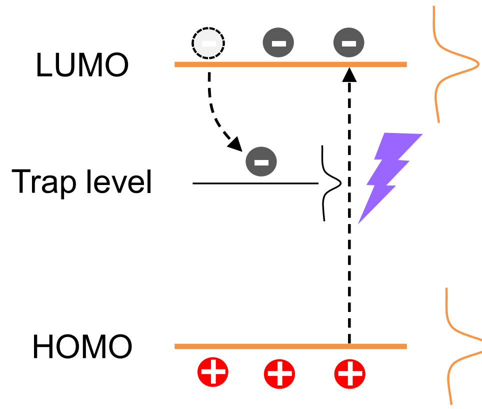

Fig. S17 The schematic diagram of the permanent trapping of photogenerated electrons in oxygen-induced deep trapping levels of the 2DMCs under light illumination in ambient air.

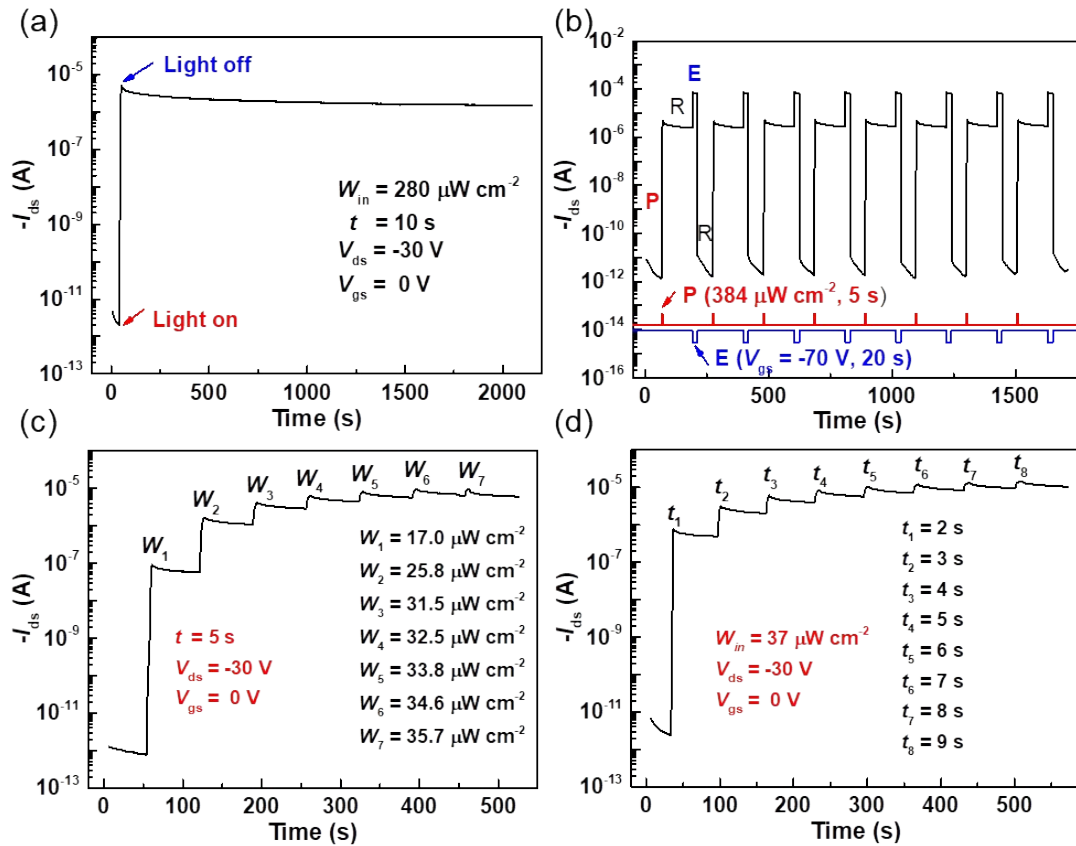

Fig. S18 Memory function of the AVMs based on a thick crystal. (All tests were performed at V_{ds} = -30 V). (a) Retention time of the AVMs (V_{gs} = 0 V, 280 μW cm^{-2} for 10 s). (b) P/E cycling characteristics of the AVMs. Each cycle includes: (i) programming (P) by a 365-nm laser pulse (V_{gs} = 0 V, 384 μW cm^{-2} for 5 s), (ii) reading (R) of high conductivity state (V_{gs} = 0 V), (iii) erasing (E) by a negative V_{gs} (V_{gs} = -70 V for 20 s), and (iv) reading (R) of low conductivity state (V_{gs} = 0 V). (c) Multiple distinct levels obtained by laser irradiation of different intensities (V_{gs} = 0 V, laser irradiation for 5 s). (d) Multiple distinct current levels obtained by laser irradiation of different time (laser power intensity fixed at 37 μW cm^{-2}, V_{gs} = 0 V).

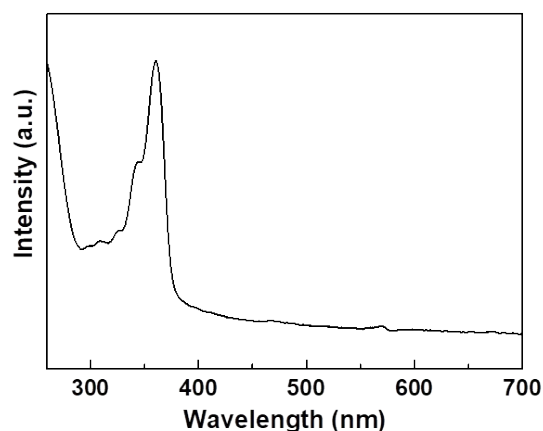

Figure S19 UV-vis absorption of 2DMCs of C8-BTBT.

Table S1 Summary of figures of merit of organic AVMs.

Organic semiconductors	Mobility ($cm^2\ V^{-1}\ s^{-1}$)	*P*	*R* (A W^{-1})	Memory window (V)	Memory ratio	Retention time (s)	Refs
Pentacene (TF,40 nm)	2.74	N/A	N/A	22	5×10^6	$>2\times10^4$	[6]
Pentacene (TF, 45 nm)	0.3	2.8×10^3	2.19	7.8	6.7×10^4	$>10^4$	[7]
Pentacene (TF, 40 nm)	1.1	N/A	N/A	16	$>10^6$	$>10^4$	[8]
PTCDI-$C_{13}H_{27}$ (TF, 40 nm)	0.1	N/A	N/A	~8	$>10^5$	$>10^4$	[8]
Pentacene (TF, 40 nm)	0.5	N/A	N/A	~7	$\sim10^4$	$>10^3$	[9]
Pentacene (TF, 40 nm)	0.34	N/A	N/A	15	$>10^4$	$>10^3$	[10]
Pentacene (TF, 50 nm)	N/A	6.5×10^3	9×10^1	42	$>10^4$	$>10^4$	[11]
Pentacene (TF, 40 nm)	0.4	N/A	N/A	~30	$>10^6$	$>10^4$	[12]
Pentacene (TF, 50 nm)	0.13	$\sim1.8\times10^4$	9.4×10^2	~56	$\sim5\times10^4$	$>10^4$	[13]
Pentacene (TF)	N/A	1.92×10^6	4.5×10^1	37.2	$\sim10^5$	$>10^4$	[14]
Pentacene (TF, 100 nm)	N/A	N/A	7×10^2	~18	N/A	$>10^4$	[15]
PCDTPT (TF, 120 nm)	N/A	$>2\times10^2$	1.04×10^2	73	7×10^4	$>10^4$	[16]
Pentacene (TF, 50 nm)	0.28	N/A	1×10^{-3}	6.7	$>10^4$	$>4\times10^4$	[17]
Pentacene (TF, 50 nm)	1.23	N/A	3.8×10^{-5}	8.2	1.67×10^3	$>10^3$	[18]
Pentacene (TF, 50 nm)	1.77	N/A	1.45×10^{-2}	31.5	3.9×10^5	$>10^3$	[18]
Pentacene (TF, 50 nm)	5.51	N/A	3.13×10^{-1}	41.1	8.64×10^5	$>10^3$	[18]
Pentacene (TF, 50 nm)	2.53	N/A	1.07×10^{-1}	39.5	5.95×10^5	$>10^3$	[18]
C10-DNTT (TF, 30 nm)	1.0	10^5	5×10^{-1}	15.08	$\sim10^3$	$>2\times10^4$	[19]
Pentacene (TF, 50 nm)	8.2×10^{-3}	N/A	N/A	19.7	3.1×10^3	$>10^4$	[20]
BBTNDT (TF, 40 nm)	7.7	2.87×10^6	4.33×10^2	60	$>10^6$	$>2\times10^4$	[21]
C8-BTBT (2DMC, 17 nm)	17.1	1.5×10^{10}	2.3×10^5	61.5	$>10^7$	$>1\times10^4$	This work

TF is short for thin film.

Table S2 Summary of figures of merit of OPDs.

Organic semiconductors	Mobility ($cm^2\ V^{-1}\ s^{-1}$)	*P*	*R* (A W^{-1})	Refs
Me-ABT (SC)	1.66	1×10^4	1.2×10^4	[22]
A-EHDTT (SC)	1.6	1.4×10^5	1.4×10^4	[23]
PY 4(THB) (SC)	0.7	1.2×10^6	2×10^3	[24]
BBDTE (SC)	1.62	1×10^5	9.8×10^3	[25]
p-DTS(FBTTH$_2$)$_2$ (SC)	1.8	1×10^4	3×10^3	[26]
TFT-CN (SC)	1.36	5×10^5	9×10^4	[27]
TIPS-Pentacene (SC)	2.06	1.36×10^8	8.45×10^2	[28]
C6-DPA (SC)	1.81	8.8×10^7	2.63×10^2	[29]
1,6-DTEP (SC)	2.1	1.6×10^5	2.86×10^6	[30]
2,7-DTEP (SC)	2.1	4.35×10^3	1.04×10^5	[30]
Pentacene (TF)	0.49	1×10^5	5×10^1	[31]
6T (TF)	0.09	1.3×10^3	2.4	[32]
ABT (TF)	0.4	1×10^3	8×10^3	[33]
F$_{16}$CuPc (TF)	5.3×10^{-4}	2.2×10^1	1.5×10^{-3}	[34]
P3HT (TF)	0.07	3.8×10^3	2.5×10^2	[35]
TIPS-Pentacene (TF)	0.02	1×10^7	N/A	[36]
DPA (TF)	12	8.5×10^7	1.34×10^5	[37]
C8-BTBT (2DMC)	17.1	1.5×10^{10}	2.3×10^5	This Work

SC is short for single crystal and TF is short for thin film.

The reliability of the storage states is evaluated by comparing the gaps of two neighboring states and their noise.[38] The gap between the two states should be greater than the sum of their standard deviation (STD) so that the two states can be distinguished. The formula of the gap to STD sum ratio is:

$$Ratio = \frac{I_{store}(n+1) - I_{store}(n)}{STD(n+1) + STD(n)}$$

where n = 1, 2, 3.... . By substituting the storage currents and STD of different neighboring states in the formula, the ratio can be calculated. When the ratio is larger than 1, it indicates that the two states are distinguished from each other. The reliability of other states is evaluated by the same method, where the result is plotted in Table S3 and S4 of the supplementary information. All ratios are greater than 1, which indicates that all storage states are valid.

Table S3 Gap to STD ratio for all the storage states of Fig. 3c.

n	I_{store}(n+1) (A)	I_{store}(n) (A)	STD(n+1) (A)	STD(n) (A)	Ratio
1	4.37×10^{-7}	9.39×10^{-8}	2.6107×10^{-8}	1.2589×10^{-7}	8.86
2	7.68×10^{-7}	4.37×10^{-7}	4.3548×10^{-8}	2.6107×10^{-8}	4.75
3	1.14×10^{-6}	7.68×10^{-7}	6.7021×10^{-8}	4.3548×10^{-8}	3.36
4	1.66×10^{-6}	1.14×10^{-6}	1.0301×10^{-7}	6.7021×10^{-8}	3.06
5	2.32×10^{-6}	1.66×10^{-6}	1.4385×10^{-7}	1.0301×10^{-7}	2.67
6	3.15×10^{-6}	2.32×10^{-6}	1.8888×10^{-7}	1.4385×10^{-7}	2.49
7	4.17×10^{-6}	3.15×10^{-6}	2.5355×10^{-7}	1.8888×10^{-7}	2.31
8	5.32×10^{-6}	4.17×10^{-6}	3.1412×10^{-7}	2.5355×10^{-7}	2.03
9	6.53×10^{-6}	5.32×10^{-6}	3.6061×10^{-7}	3.1412×10^{-7}	1.79

Table S4 Gap to STD ratio for all the storage states of Fig. 3d.

n	I_{store}(n+1) (A)	I_{store}(n) (A)	STD(n+1) (A)	STD(n) (A)	Ratio
1	1.35×10^{-7}	2.92×10^{-8}	9.8446×10^{-9}	3.8050×10^{-9}	7.75
2	2.98×10^{-7}	1.35×10^{-7}	1.5435×10^{-8}	9.8446×10^{-9}	6.45
3	5.33×10^{-7}	2.98×10^{-7}	2.8310×10^{-8}	1.5435×10^{-8}	5.37
4	8.52×10^{-7}	5.33×10^{-7}	4.6457×10^{-8}	2.8310×10^{-8}	4.27
5	1.19×10^{-6}	8.52×10^{-7}	1.6347×10^{-7}	4.6457×10^{-8}	1.61
6	1.76×10^{-6}	1.19×10^{-6}	1.2585×10^{-7}	1.6347×10^{-7}	1.97
7	2.20×10^{-6}	1.76×10^{-6}	1.6759×10^{-7}	1.2585×10^{-7}	1.50
8	3.16×10^{-6}	2.20×10^{-6}	2.3195×10^{-7}	1.6759×10^{-7}	2.40

9	4.07×10^{-6}	3.16×10^{-6}	2.9308×10^{-7}	2.3195×10^{-7}	1.73

REFERENCES

1. J. J. Brondijk, W. S. Roelofs, S. G. Mathijssen, A. Shehu, T. Cramer, F. Biscarini, P. W. Blom and D. M. de Leeuw, *Phys. Rev. Lett.*, 2012, **109**, 056601.
2. D. Kufer and G. Konstantatos, *ACS Photonics*, 2016, **3**, 2197-2210.
3. Q. Wang, J. Qian, Y. Li, Y. Zhang, D. He, S. Jiang, Y. Wang, X. Wang, L. Pan, J. Wang, X. Wang, Z. Hu, H. Nan, Z. Ni, Y. Zheng and Y. Shi, *Adv. Funct. Mater.*, 2016, **26**, 3191-3198.
4. A. Shehu, S. D. Quiroga, P. D'Angelo, C. Albonetti, F. Borgatti, M. Murgia, A. Scorzoni, P. Stoliar and F. Biscarini, *Phys. Rev. Lett.*, 2010, **104**, 246602.
5. F. Dinelli, M. Murgia, P. Levy, M. Cavallini, F. Biscarini and D. M. de Leeuw, *Phys. Rev. Lett.*, 2004, **92**, 116802.
6. L. Zhang, T. Wu, Y. Guo, Y. Zhao, X. Sun, Y. Wen, G. Yu and Y. Liu, *Sci. Rep.*, 2013, **3**, 1080.
7. X. Liu, H. Zhao, G. Dong, L. Duan, D. Li, L. Wang and Y. Qiu, *ACS Appl. Mater. Interfaces*, 2014, **6**, 8337-8844.
8. Z.-D. Zhang, X. Gao, Y.-N. Zhong, J. Liu, L.-X. Zhang, S. Wang, J.-L. Xu and S.-D. Wang, *Adv. Electron. Mater.*, 2017, **3**, 1700052.
9. Y.-N. Zhong, X. Gao, J.-L. Xu, H. Sirringhaus and S.-D. Wang, *Adv. Electron. Mater.*, 2019, **6**, 1900955.
10. L.-X. Zhang, X. Gao, J.-J. Lv, Y.-N. Zhong, C. Xu, J.-L. Xu and S.-D. Wang, *ACS Appl. Mater. Interfaces*, 2019, **11**, 40366-40371.
11. S.-W. Cheng, T. Han, T.-Y. Huang, Y.-H. Chang Chien, C.-L. Liu, B. Z. Tang and G.-S. Liou, *ACS Appl. Mater. Interfaces*, 2018, **10**, 18281-18288.
12. J.-J. Lv, X. Gao, L.-X. Zhang, Y. Feng, J.-L. Xu, J. Xiao, B. Dong and S.-D. Wang, *Appl. Phys. Lett.*, 2019, **115**, 113302.
13. M. Kang, A.-N. Cha, S.-A. Lee, S.-K. Lee, S. Bae, D.-Y. Jeon, J.-M. Hong, S. Fabiano, M. Berggren and T.-W. Kim, *Org. Electron.*, 2020, **78**, 105554.
14. T.-Y. Huang, C.-H. Chen, C.-C. Lin, Y.-J. Lee, C.-L. Liu and G.-S. Liou, *J. Mater. Chem. C*, 2019, **7**, 11014-11021.
15. S. Jang, E. Hwang, Y. Lee, S. Lee and J. H. Cho, *Nano Lett.*, 2015, **15**, 2542-2547.
16. X. Wu, S. Lan, D. Hu, Q. Chen, E. Li, Y. Yan, H. Chen and T. Guo, *J. Mater. Chem. C*, 2019, **7**, 9229-9240.
17. J.-Y. Chen, Y.-C. Chiu, Y.-T. Li, C.-C. Chueh and W.-C. Chen, *Adv. Mater.*, 2017, **29**, 1702217.
18. E. Ercan, J.-Y. Chen, C.-C. Shih, C.-C. Chueh and W.-C. Chen, *Nanoscale*, 2018, **10**, 18869-18877.

19. T. Xu, S. Guo, W. Qi, S. Li, M. Xu and W. Wang, *ACS Appl. Mater. Interfaces*, 2020, **12**, 21952-21960.
20. L. Zhou, S.-T. Han, S. Shu, J. Zhuang, Y. Yan, Q.-J. Sun, Y. Zhou and V. A. L. Roy, *ACS Appl. Mater. Interfaces*, 2017, **9**, 34101-34110.
21. K. Pei, X. Ren, Z. Zhou, Z. Zhang, X. Ji and P. K. L. Chan, *Adv. Mater.*, 2018, **30**, 1706647.
22. Y. Guo, C. Du, G. Yu, C.-a. Di, S. Jiang, H. Xi, J. Zheng, S. Yan, C. Yu, W. Hu and Y. Liu, *Adv. Funct. Mater.*, 2010, **20**, 1019-1024.
23. K. H. Kim, S. Y. Bae, Y. S. Kim, J. A. Hur, M. H. Hoang, T. W. Lee, M. J. Cho, Y. Kim, M. Kim, J.-I. Jin, S.-J. Kim, K. Lee, S. J. Lee and D. H. Choi, *Adv. Mater.*, 2011, **23**, 3095-3099.
24. Y. S. Kim, S. Y. Bae, K. H. Kim, T. W. Lee, J. A. Hur, M. H. Hoang, M. J. Cho, S.-J. Kim, Y. Kim, M. Kim, K. Lee, S. J. Lee and D. H. Choi, *Chem. Commun.*, 2011, **47**, 8907-8909.
25. G. Zhao, J. Liu, Q. Meng, D. Ji, X. Zhang, Y. Zou, Y. Zhen, H. Dong and W. Hu, *Adv. Electron. Mater.*, 2015, **1**, 1500071.
26. Q. Cui, Y. Hu, C. Zhou, F. Teng, J. Huang, A. Zhugayevych, S. Tretiak, T.-Q. Nguyen and G. C. Bazan, *Adv. Funct. Mater.*, 2018, **28**, 1702073.
27. C. Wang, X. Ren, C. Xu, B. Fu, R. Wang, X. Zhang, R. Li, H. Li, H. Dong, Y. Zhen, S. Lei, L. Jiang and W. Hu, *Adv. Mater.*, 2018, **30**, 1706260.
28. Y. Zhang, X. Zhu, S. Yang, F. Zhai, F. Zhang, Z. Niu, Y. Feng, W. Feng, X. Zhang, L. Li, R. Li and W. Hu, *Nanoscale*, 2019, **11**, 12781-12787.
29. J. Yao, Y. Zhang, X. Tian, X. Zhang, H. Zhao, X. Zhang, J. Jie, X. Wang, R. Li and W. Hu, *Angew. Chem. Int. Ed.*, 2019, **58**, 16082-16086.
30. J. Tao, D. Liu, Z. Qin, B. Shao, J. Jing, H. Li, H. Dong, B. Xu and W. Tian, *Adv. Mater.*, 2020, **32**, 1907791.
31. Y.-Y. Noh, D.-Y. Kim and K. Yase, *J. Appl. Phys.*, 2005, **98**, 074505.
32. Y.-Y. Noh, J. Ghim, S.-J. Kang, K.-J. Baeg, D.-Y. Kim and K. Yase, *J. Appl. Phys.*, 2006, **100**, 094501.
33. Y. Guo, C. Du, C.-a. Di, J. Zheng, X. Sun, Y. Wen, L. Zhang, W. Wu, G. Yu and Y. Liu, *Appl. Phys. Lett.*, 2009, **94**, 143303.
34. B. Mukherjee, M. Mukherjee, Y. Choi and S. Pyo, *J. Phys. Chem. C*, 2009, **113**, 18870–18873.
35. T. Pal, M. Arif and S. I. Khondaker, *Nanotechnol.*, 2010, **21**, 325201.
36. Y.-H. Kim, J.-I. Han, M.-K. Han, J. E. Anthony, J. Park and S. K. Park, *Org. Electron.*, 2010, **11**, 1529-1533.
37. D. Ji, T. Li, J. Liu, S. Amirjalayer, M. Zhong, Z. Y. Zhang, X. Huang, Z. Wei, H. Dong, W. Hu and H. Fuchs, *Nat. Commun.*, 2019, **10**, 12.
38. D. Xiang, T. Liu, J. Xu, J. Y. Tan, Z. Hu, B. Lei, Y. Zheng, J. Wu, A. H. C. Neto, L. Liu and W. Chen, *Nat. Commun.*, 2018, **9**, 2966.